Lasers in Medical Science
https://doi.org/10.1007/s10103-019-02888-0

ORIGINAL ARTICLE

Correlation between light absorbance and skin color using fabricated skin phantoms with different colors

Hang Chan Jo[1] · Dae Yu Kim[1]

Received: 25 May 2019 / Accepted: 23 September 2019

Abstract
The objective of this study is to investigate the need for detailed classification of skin colors through the quantification of skin color and light absorbance differences. Skin color is one of the most important factors in dermatological laser treatments. Dermatological laser treatments are currently performed based on the experience and judgment of the doctor with the Fitzpatrick scale. However, the Fitzpatrick scale and the doctor's experience were not quantified assessment methods for skin color classification and laser parameters selection. Improper selection of laser irradiating parameters can lead to undesirable tissue effects and treatment outcomes. We analyzed the correlations between absorbance and quantified colors using skin phantoms to identify that using the Fitzpatrick scale in dermatological treatments have limitations. Absorbance differences for different skin colors are measured at 532 nm with a custom-built system for radiant power measurements using skin phantoms fabricated with nine different colors. Some correlations between the color and absorbance agree with the Fitzpatrick scale. Generally, absorbance for the bright colored phantoms is lower than that for the darker colored phantoms. However, some phantoms fabricated with bright colors exceptionally have higher absorbance than those with darker colors. This means that for conventional standards, the Fitzpatrick scale may not always be accurate at 532-nm lights. Through these experiments, we demonstrate the need for a reliable classification standard for skin colors based on quantification of the skin colors and absorbance differences for each skin color as an alternative to the Fitzpatrick scale, which has limitations at certain wavelengths.

Keyword Absorbance of skin · Skin phantom · Skin color · Fitzpatrick scale · Absorbance differences by skin color

Introduction

Dermatological laser treatments are frequently used for skin resurfacing and hair, tattoo, and pigment removals. However, side effects such as post-inflammatory hyperpigmentation, post-inflammatory hypopigmentation, blisters, erythema, and hemorrhage are not uncommon [1–3]. These side effects result from collateral thermal damage at the periphery of the laser target area by heat accumulation. The case that the absorbed laser energy was larger than the released thermal energy was mainly responsible for the heat accumulation [4]. The characteristics of the skin including the colors, structures, and composition as well as the output power and pulse durations of the laser devices are the factors that affect heat accumulation. Skin color had a direct correlation with the absorption of light because the chromophores in skin such as melanin and heme are the main absorbers of light [5]. Differences in the skin color of each person were caused by deviations in the composition ratios of these chromophores [6]. Although the characteristics of irradiated skin are also important factors for heat accumulation, previous studies were only focused on laser parameters without considering skin characteristics. For example, research involving the modulation of pulse duration demonstrated that shorter pulse durations prevented heat accumulation and negative side effects [7–11]. However, studies investigating the interaction between skin color differences and certain laser parameters are relatively insufficient at preventing heat accumulation and side effects compared with those researches involving the modulation of laser parameters. Previous studies and treatments classified skin colors according to the Fitzpatrick scale and the experiences of the medical doctor without quantitative analysis [12].

The Fitzpatrick scale was a numerical classification schema with six possible classifications for human skin types depending

✉ Dae Yu Kim
dyukim@inha.ac.kr

[1] Electrical Engineering, Inha University, 100 Inha-ro, Michuhol-gu, Incheon 22212, Korea

Published online: 30 October 2019

on the response to ultraviolet light [13]. The Fitzpatrick scale is a widely used method to classify skin types including skin colors even though the criteria for the classification of skin colors have been not quantitatively established. In this regard, the actual colors used with the Fitzpatrick scales are variable. Irregular standards of color classifications can lead to errors due to the arbitrary grouping of ambiguous colors. In addition, the Fitzpatrick scale has limitations for use in dermatological laser treatments because the wavelengths of the laser used for skin treatments differ from that of ultraviolet light. Lasers operated at 532 nm and 1064 nm were usually used for dermatological procedures [14–16]. Therefore, analysis of the correlations between quantified skin colors and absorbance at specific wavelengths is necessary to minimize the probability of side effects through accurate assessment of skin states and laser irradiating parameters.

Experimental models with controlled characteristics such as thickness, scattering, and structure are required to investigate correlations between absorbance and quantified skin colors. Previous studies mostly used light irradiation to the tissues of animals and patients for the investigation of light-tissue interactions [7–11, 14–17]. However, these methods had limitations regarding the control of experimental conditions because in vivo and ex vivo experimental models have individual characteristics including skin colors as well as structure differences such as the existence of pores and sweat glands at the light-irradiated area. Deviations in these characteristics are uncontrollable and can impair accurate measurements. On the other hand, artificial experimental models in the form of phantoms produced using constant fabrication methods and materials can be used to control experimental conditions, leading to accurate results uninfluenced by disturbance. Tissue phantoms with the desired characteristics have been used as testing models by many researchers and developers to evaluate the performance of systems and establish the reliability of theoretical models [18–22]. A previous study by Lualdi et al. was performed using skin phantoms made with silicone rubber with different concentrations of a cosmetic powder that had one skin color [23]. Phantoms made using one-color cosmetic powder with different concentrations have limitations in mimicking various types of skin color expressed by various chromophores including melanin and heme. In addition, the main chromophore for skin color, melanin, was categorized into three basic types: eumelanin, pheomelanin, and neuromelanin. The most common type, eumelanin, was also separated into two subtypes of brown and black eumelanin [24]. Skin phantoms fabricated with chromophores with various colors would be ideal models for investigating absorbance differences depending on skin color.

In this study, we fabricate skin phantoms and measure the attenuation of light in the phantoms to calculate absorbance. Our phantoms are fabricated using nine color cosmetic powders to mimic tissue models with various skin colors. The characteristics of the phantoms other than the color are controlled using a constant fabrication process and materials. The radiant power for each phantom is measured using a continuous wave (CW) laser at 532 nm with an optical power meter. Through these experiments, we perform measurement absorbance differences for different skin colors and confirmed the limitations of the Fitzpatrick scale. This research represents an initial step in the development of a technique that can provide optimal laser irradiating parameters for dermatological laser treatments through the prediction of personalized absorbance based on skin color measurement.

Materials and methods

Materials of phantoms

Pourable and addition-curing two-part silicone rubber (Elastosil RT604 A/B, Wacker, Munich, Germany) was applied as the base material for the phantoms in this study. The silicone rubber is transparent and has a similar refractive index (1.404) to soft tissue (n = 1.33–1.50) [25]. The silicone consists of main (RT604 A) and catalyst (RT604 B) solvents. These two components were mixed at a ratio of 9:1 (RT604 A: RT604 B) by weight. Silicone rubber was also used in a previous research by Lualdi et al. [23]. Cosmetic skin powders (Sheer Finish Pressed Powder, Bobbi Brown, New York, USA) classified into nine types according to color were used as chromophores and absorbers to fabricate the phantoms. Aluminum oxide (Al_2O_3) particles (Sigma Aldrich, Saint Louis, USA) were added as an additional scattering factor to mimic the scattering capability of skin [23].

Manufacturing process

The fabrication of the phantoms was performed through the constant process shown in Fig. 1a. The mixed solutions for the phantom consisted of cosmetic powder for each color, controlled silicone, and Al_2O_3. Two groups of solutions classified by the composition ratio of the cosmetic powder were mixed to demonstrate the absorbance differences according to different concentrations of absorbers. The first phantom group consisted of Al_2O_3 particles (1.2 wt%), cosmetic powder (1.2 wt%), main silicone (RT604A, 87.84 wt%), and catalyst (RT604B, 9.76 wt%). The second phantom group consisted of Al_2O_3 particles (1.2 wt%), cosmetic powder (5.0 wt%), main silicone (RT604A, 84.42 wt%), and catalyst (RT604B, 9.38 wt%). The list for composition ratio of each phantom is written in Table 1. A homogenizer (HG-15D, DAIHAN Science, Seoul, Republic of Korea) was used to create a homogeneous mixture (Fig. 1a). The homogenizer was operated at the minimum revolutions per minute (2000 rpm) for 2 min because high rpm and lengthy operation can generate heat at the rotor in the solutions. Heat in the mixture leads to early hardening, which affects the control of flatness and thickness during the fabrication process. The homogeneous mixtures were dropped onto slide glass for

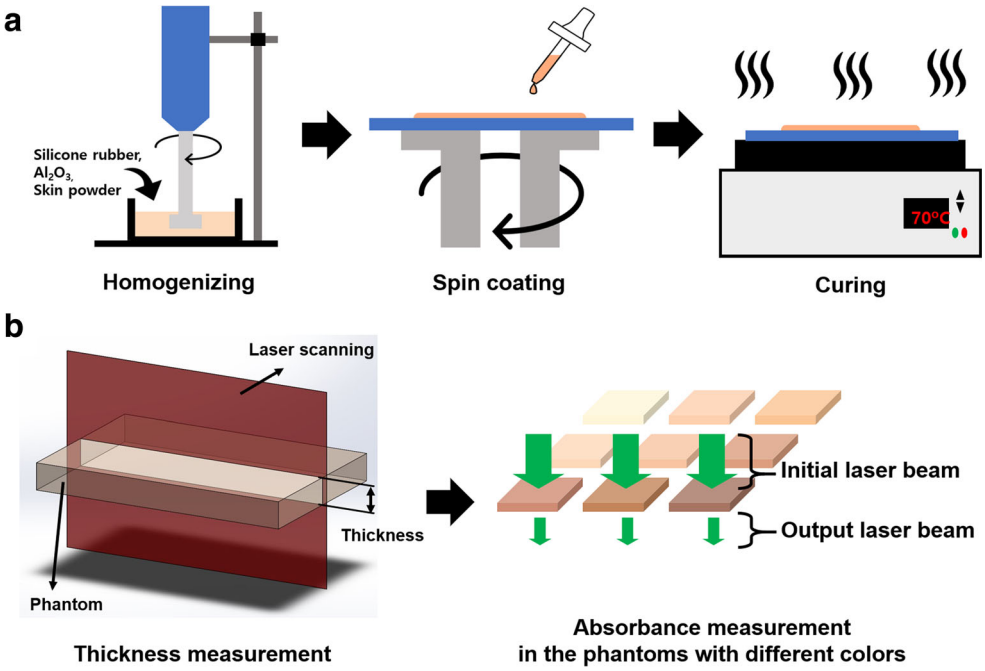

Fig. 1 Schematic of fabrication process for phantoms and measurement process for thickness and absorbance of phantoms. **a** Phantoms were fabricated through solution homogenizing, flattening using a spin coater, and curing on a hot plate at 70 °C. **b** The thickness of the phantoms was measured by calculation of the distance between the surface and bottom using cross-sectional images. Afterward, absorbance was measured based on the correlation between the initial and output laser beams

spin coating (Fig.1a). The slide glasses were fixed on the chuck of a spin coater using a vacuum pump. The spin coater was used to fabricate thickness-controlled and uniform surface phantoms. The spin coater was operated under two parameters for the rpm levels and running time. The chuck of the spin coater was rotated under 200 rpm for 30 s with the solutions for the first phantom group (content of cosmetic powder: 1.2 wt%). The second phantom group (cosmetic powder content: 5.0 wt%) was treated under 250 rpm for 40 sec. These parameters for the spin coater operations were obtained through several working tests. Homogenized mixtures were immediately cured for 3 min on a hot plate (Fig. 1a) at a temperature of 70 °C. This temperature was sufficient to cure the solutions for the phantoms according to the technical datasheet for silicone, which stated that a temperature of 70 °C for 30 min can cure a solution with a thickness of 1 cm. All phantoms (394.3 ± 45.7 μm) were thinner than 1 mm.

Measurements

Cross-sectional images of the phantoms acquired using a custom-built swept source-optical coherence tomography (SS-OCT) system were used to evaluate the thickness and flatness of the fabricated phantoms. OCT is a useful and powerful tool for obtaining tomograms, cross-sectional images, and volume images of targets in the industrial process and medical fields such as Dermatology, Dentistry, and Ophthalmology [26–35]. The SS-OCT system used in these experiments included a high-speed wavelength swept laser (Axsun, BILLERICA, MA) as a light source. The swept source laser had a sweeping rate of 50 kHz and a 110 bandwidth with a center wavelength of 1310 nm.

The absorbance of the phantoms was calculated using Beer-Lambert's Law, which is a theory used to calculate absorbance through the attenuation of light in light-traveling materials. The correlations of the parameters defined in Beer-Lambert's Law can be expressed as follows:

$$A = \varepsilon lc = \log_{10}\frac{I_0}{I} \quad (1)$$

where

A: absorbance, normally called the optical density,

ε: absorptivity or molar attenuation coefficient in the material samples,

Table 1 Composition ratio of each phantom group

Phantom groups by composition ratio of cosmetic powders	Phantoms (n=1, 2, , 9)	Main silicon (RT604 A)	Catalyst (RT604 B)	Aluminum oxide	Cosmetic powder with skin color
1.2 wt% group	C[n]P	87.84 wt%	9.76 wt%	1.2 wt%	1.2 wt%
5.0 wt% group	C[n]P	84.42 wt%	9.38 wt%	1.2 wt%	50.wt%

l: path length of the beam or thickness of the material samples,

c: amount concentration of the material samples,

I_0: radiant flux, unit (Watts), initial radiant power of light,

I: radiant flux, unit (Watts), transmitted radiant power of light.

A fiber-coupled CW laser (CNI laser, Changchun, China) was irradiated to measure I_0 and I. The specifications of the laser included a maximum power of 1 Watt with a 532-nm wavelength. The radiant flux, I_0 and I, was measured using an optical power meter with a Si photodiode detector (PM200 with S120C, Thorlabs, Newton, NJ, USA). A neutral density filter (optical density: 0.1) was used to support the phantoms in the measurement mount. The initial radiant power I_0 was measured without phantoms. After measuring the initial and transmitted radiant power, the absorbance was calculated using Eq. (1). In addition, calibrated absorbance was calculated to compensate thickness deviations in the phantom using Eq. (2).

$$A_{cali} = \mathrm{A} \times \frac{l_{cont}}{l_{mea}} \tag{2}$$

where

A_{cali}: calibrated absorbance,

l_{cont}: control thickness of phantom,

l_{mea}: measured thickness of phantoms.

Table 2 RGB values and phototypes of the Fitzpatrick scale

The Fitzpatrick scale and phototypes	Red (0~255)	Green (0~255)	Blue (0~255)
FS1 (Type Ⅰ)	254	254	254
FS2 (Type Ⅱ)	251	238	210
FS3 (Type Ⅲ)	234	205	121
FS4 (Type Ⅳ)	215	163	6
FS5 (Type Ⅴ)	150	115	78
FS6 (Type Ⅵ)	110	59	7

Results

We fabricate skin phantoms with two concentration groups (1.2 wt% and 5.0 wt%) by controlling the cosmetic powder content using nine different colors. All parameters for the materials in the phantoms are controlled except for the content and type of cosmetic powder. The colors of the cosmetic powders are quantified to RGB values by analyzing the color images provided by the powder manufacturer. To extract the RGB values, the 3D color inspector plugin for Image J (NIH) is used. The RGB values for each color type in the Fitzpatrick scale are also extracted from an image in a previous study using ImageJ because validated RGB values for the Fitzpatrick scale do not exist. The quantified RGB values for each color are shown in Fig. 2b, Table 2, and Table 3. The coverage of the colors used in phantom fabrication is presented based on the distribution of powder colors located between each color type on the Fitzpatrick scale.

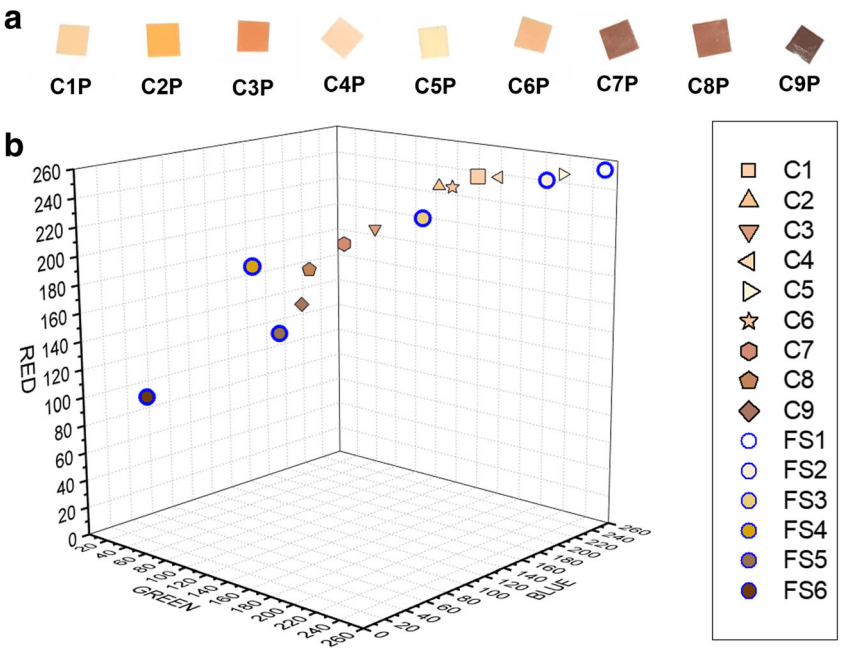

Fig. 2 Fabricated skin phantoms and color distributions of the cosmetic powders. **a** Images of the skin phantoms. C[n]P stands for Color [n] Phantom with C[n] color skin powder (n = 1, 2, …, 9). **b** The colors of the cosmetic powder and Fitzpatrick scale. FS[k] is Fitzpatrick scale k (k = 1, 2,…, 6)

Table 3 RGB values of colors used for phantoms

Colors of cosmetic powders	Red (0~255)	Green (0~255)	Blue (0~255)
C1	255	208	174
C2	251	197	147
C3	220	158	127
C4	255	246	217
C5	254	217	185
C6	248	196	162
C7	209	140	116
C8	195	133	89
C9	167	117	98

Cross-sectional scan images of OCT are used to acquire the thickness of the fabricated phantoms (Fig. 3). The measured thickness for each phantom is used to compensate for the thickness difference in absorbance calculation. The thickness of the phantoms is calculated by counting the pixels (5.7 μm × 5.7 μm) between the surface and bottom in cross-sectional images. Deviations in thickness (394.3 ± 45.7 μm) are measured, even though the fabrication process and materials are controlled. These deviations attribute to quantify the differences in solution droplets and position differences with the axis of rotation due to the manual dropping process. In addition, cross-sectional images are used to evaluate the flatness of the structure in the fabricated phantoms. If the materials were agglomerated or weighted toward an arbitrary position during the fabrication process, the scattering pattern and structure would be irregularly distorted. The cross-sectional images of the phantom show a uniform surface and structure without distortion (Fig. 3).

Measurements of the initial and transmitted radiant power with the 532-nm CW laser are repeated three times to calculate the absorbance of the phantoms using the custom-built system using the optical power meter (Fig. 4a, b). The absorbance of the phantoms is calculated with Beer-Lambert's Law presented in Eq. (1) using the measured values for the light attenuation and thickness of the phantoms. After calculating the absorbance, the influence of thickness variation is compensated with Eq. (2). Thickness calibration is performed under the assumption that the thickness is linear regarding the absorbance without measurement errors, followed by analysis of the correlations between absorbance and quantified colors for each phantom. The compensated absorbance A_{cali} for the phantoms is shown in Fig. 4c.

The absorbance differences for different phantom colors are irregular. Phantom C5P have higher absorbance than C1P, C2P, C3P, and C4P even though C5P have the lightest color among the fabricated phantoms. C4P have higher absorbance than C1P; however, the colors of C1P and C4P are similar. In addition, similar absorbance is observed for C2P and C3P as well as for C4P and C5P even though these phantoms have different colors. Irregular correlations between the absorbance and colors of the phantoms are expected due to differences in reflexibility depending on the phantom color and variations in the absorptivity for each value of RGB at 532 nm. However, the phantom with darker colors have higher absorbance than those with lighter colors. C7P, C8P, and C9P show higher absorbance than the others. These aspects agree with the Fitzpatrick scales. The absorbance for the higher content group (5.0 wt% concentration) is higher than that for the lower content group (1.2 wt% concentration). These correlations between the absorbance and the concentration of the absorber have also been reported in previous studies on absorbance differences with different absorber concentrations.

Discussion

Although people have different skin colors by various factors such as the thickness of each layer, the composition ratio, and different types of chromophores, previous studies were performed using skin phantoms fabricated by modulating the

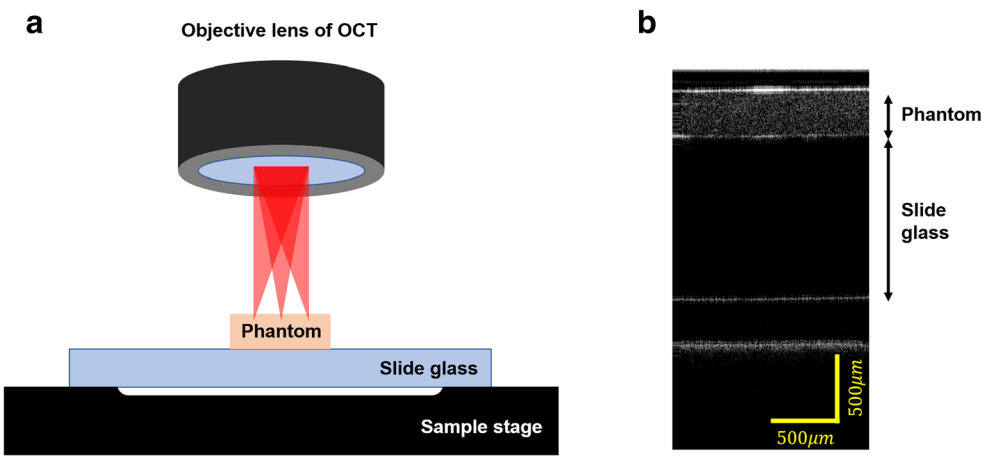

Fig. 3 Thickness measurement method. **a** Schematic of the sample arm in custom-built OCT. **b** Cross-sectional images of the phantom

concentration of chromophores using only one-color material. We expected that measuring the absorbance differences in various color phantoms would help establish optimal laser irradiating criteria and reveal the limitations of conventional methods used to categorize skin colors like the Fitzpatrick scale. We fabricate nine colored phantoms and compare the absorbance of each phantom. The results show irregular correlations between the absorbance and color of the phantoms. Different absorbance values are obtained for phantoms with similar colors (C1P and C4P) and lower values are obtained for phantoms with darker colors than those with light colors (C5P). In addition, similar absorbance values are observed for phantoms (C2P and C3P, C4P and C5P) with different colors. However, correlations in accordance with the Fitzpatrick scale are also observed in several phantoms (C7P, C8P, and C9P). These results demonstrate that detailed skin classification based on quantified data for skin color and absorbance is needed for certain wavelengths and that skin classification using unquantifiable and rough standards has limitations. Detailed skin classification based on quantified data can help determine the most effective and optimal laser irradiating criteria to minimize side effects along with previous methods like the Fitzpatrick skin scale. The limitations of this study are that the RGB values for the phantoms could not be controlled and the structure of real skin tissue was not replicated. If we can control the RGB values, we can obtain more scientific and advanced results. For example, comparison of phantom colors between Red values 125 and 190 with fixed Green and Blue values can help determine the influence of the Red value on absorbance. Second, the fabricated skin phantoms in this study comprised a single layer. However, real skin consists of four layers (stratum corneum, epidermis, dermis, and hypodermis). Each layer of real skin has a different chromophore content, different tissue composition ratios, and different thickness. For example, the dermis has blood capillaries and a thicker layer than the epidermis. Blood in capillaries means that the dermis includes more heme, which is a light absorber, than the epidermis. Multi-layer skin phantoms in which the concentration of chromophores in each layer can be controlled are required for more scientific investigation of the correlations between skin color and absorbance.

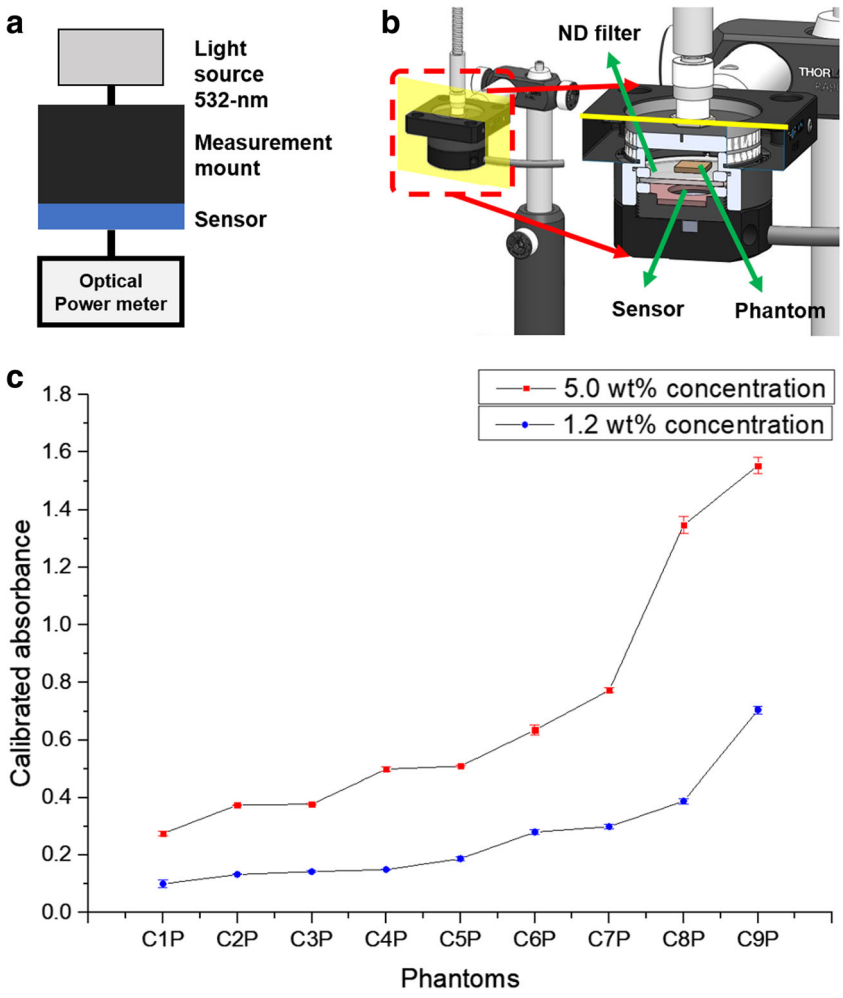

Fig. 4 The absorbance measurement system and the measured absorbance for the phantoms. **a** Schematic of the custom-built absorbance measurement system. **b** Three-dimensional and cross-sectional rendering images of the system. **c** Calibrated absorbance value for each phantom

Conclusion

In this research, we fabricate skin phantoms using cosmetic powders with nine quantified colors and investigate the absorbance differences between different colored phantoms at 532-nm lights. The results reveal the limitations of the previous skin classification standard and the necessity for fine classification based on quantified data. These experiments represent the first step in the study of optimal laser irradiating standards based on the correlations between quantified skin color and absorbance at certain wavelengths. Although we could not demonstrate the correlations between absorbance and RGB values, future experiments will complement these weaknesses through the control of RGB values. In addition, multi-layer skin phantoms will be used to create skin models that mimic real skin in our further works.

Author contributions Hang Chan Jo designed and performed the experiments, analyzed the data, and wrote the paper. Dae Yu Kim conceived and designed the experiments, supervised the work, and revised the paper.

Funding information This research was financially supported by Inha University Research Grant.

Compliance with ethical standards

Conflicts of interest The authors declare that they have no conflict of interest.

References

1. Graber EM, Tanzi EL, Alster TS (2008) Side effects and complications of fractional laser photothermolysis: experience with 961 treatments. Dermatol Surg 34(3):301–305; discussion 305-307. https://doi.org/10.1111/j.1524-4725.2007.34062.x
2. Klein A, Rittmann I, Hiller KA, Landthaler M, Baumler W (2014) An Internet-based survey on characteristics of laser tattoo removal and associated side effects. Lasers Med Sci 29(2):729–738. https://doi.org/10.1007/s10103-013-1395-1
3. Toosi P, Sadighha A, Sharifian A, Razavi GM (2006) A comparison study of the efficacy and side effects of different light sources in hair removal. Lasers Med Sci 21(1):1–4. https://doi.org/10.1007/s10103-006-0373-2
4. Knappe V, Frank F, Rohde E (2004) Principles of lasers and biophotonic effects. Photomed Laser Surg 22(5):411–417. https://doi.org/10.1089/pho.2004.22.411
5. Young AR (1997) Chromophores in human skin. Phys Med Biol 42(5):789–802. https://doi.org/10.1088/0031-9155/42/5/004
6. Jablonski NG (2012) Living color : the biological and social meaning of skin color. University of California Press, Berkeley
7. Walsh JT Jr, Deutsch TF (1988) Pulsed CO2 laser tissue ablation: measurement of the ablation rate. Lasers Surg Med 8(3):264–275
8. Walsh JT Jr, Flotte TJ, Anderson RR, Deutsch TF (1988) Pulsed CO2 laser tissue ablation: effect of tissue type and pulse duration on thermal damage. Lasers Surg Med 8(2):108–118
9. Walsh JT Jr, Flotte TJ, Deutsch TF (1989) Er:YAG laser ablation of tissue: effect of pulse duration and tissue type on thermal damage. Lasers Surg Med 9(4):314–326
10. Cummings JP, Walsh JT Jr (1993) Tissue tearing caused by pulsed laser-induced ablation pressure. Appl Opt 32(4):494–503. https://doi.org/10.1364/AO.32.000494
11. Welch AJ, Gemert MJCv (1995) Optical-thermal response of laser-irradiated tissue. Lasers, photonics, and electro-optics. Plenum Press, New York
12. Sachdeva S (2009) Fitzpatrick skin typing: applications in dermatology. Indian J Dermatol Venereol Leprol 75(1):93–96
13. Fitzpatrick TB (1988) The validity and practicality of sun-reactive skin types I through VI. Arch Dermatol 124(6):869–871. https://doi.org/10.1001/archderm.124.6.869
14. Jo HC, Kim DY (2019) Observations of in vivo laser tissue ablation in animal models with different chromophores on the skin and modulating duration per laser exposure. Lasers Med Sci 34(5):1031–1039. https://doi.org/10.1007/s10103-018-2693-4
15. Saade DS, Vashi NA (2019) Treatment of purpura with Nd:YAG laser in skin types IV-VI. J Am Acad Dermatol 80(4):e73–e74. https://doi.org/10.1016/j.jaad.2018.09.003
16. Vachiramon V, Iamsumang W, Triyangkulsri K (2018) Q-switched double frequency Nd:YAG 532-nm nanosecond laser vs. double frequency Nd:YAG 532-nm picosecond laser for the treatment of solar lentigines in Asians. Lasers Med Sci 33(9):1941–1947. https://doi.org/10.1007/s10103-018-2560-3
17. Kaya TI, Guvenc U (2019) Long pulse 1,064-nm neodymium-doped yttrium aluminum garnet laser in aesthetic dermatology. Dermatol Ther 32(3):e12907. https://doi.org/10.1111/dth.12907
18. Iizuka MN, Sherar MD, Vitkin IA (1999) Optical phantom materials for near infrared laser photocoagulation studies. Lasers Surg Med 25(2):159–169
19. Martensson M, Bjallmark A, Brodin LA (2011) Evaluation of tissue Doppler-based velocity and deformation imaging: a phantom study of ultrasound systems. Eur J Echocardiogr 12(6):467–476. https://doi.org/10.1093/ejechocard/jer056
20. Remmert G, Biederer J, Lohberger F, Fabel M, Hartmann GH (2007) Four-dimensional magnetic resonance imaging for the determination of tumour movement and its evaluation using a dynamic porcine lung phantom. Phys Med Biol 52(18):N401–N415. https://doi.org/10.1088/0031-9155/52/18/N02
21. Schulten-Wijman MJ, Struijk PC, Brezinka C, De Jong N, Steegers EA (2008) Evaluation of volume vascularization index and flow index: a phantom study. Ultrasound Obstet Gynecol 32(4):560–564. https://doi.org/10.1002/uog.6112
22. Wang D, Strugnell W, Cowin G, Doddrell DM, Slaughter R (2004) Geometric distortion in clinical MRI systems Part I: evaluation using a 3D phantom. Magn Reson Imaging 22(9):1211–1221. https://doi.org/10.1016/j.mri.2004.08.012
23. Lualdi M, Colombo A, Farina B, Tomatis S, Marchesini R (2001) A phantom with tissue-like optical properties in the visible and near infrared for use in photomedicine. Lasers Surg Med 28(3):237–243. https://doi.org/10.1002/lsm.1044
24. Thody AJ, Higgins EM, Wakamatsu K, Ito S, Burchill SA, Marks JM (1991) Pheomelanin as well as eumelanin is present in human epidermis. J Invest Dermatol 97(2):340–344. https://doi.org/10.1111/1523-1747.ep12480680
25. Bolin FP, Preuss LE, Taylor RC, Ference RJ (1989) Refractive index of some mammalian tissues using a fiber optic cladding method. Appl Opt 28(12):2297–2303. https://doi.org/10.1364/AO.28.002297
26. Hsieh YS, Ho YC, Lee SY, Chuang CC, Tsai JC, Lin KF, Sun CW (2013) Dental optical coherence tomography. Sensors (Basel) 13(7):8928–8949. https://doi.org/10.3390/s130708928
27. Kim DY, Fingler J, Zawadzki RJ, Park SS, Morse LS, Schwartz DM, Fraser SE, Werner JS (2012) Noninvasive imaging of the foveal avascular zone with high-speed, phase-variance optical coherence tomography. Invest Ophthalmol Vis Sci 53(1):85–92. https://doi.org/10.1167/iovs.11-8249

28. Kim DY, Fingler J, Zawadzki RJ, Park SS, Morse LS, Schwartz DM, Fraser SE, Werner JS (2013) Optical imaging of the chorioretinal vasculature in the living human eye. Proceedings of the National Academy of Sciences 110(35):14354–14359. https://doi.org/10.1073/pnas.1307315110
29. Kim DY, Werner JS, Zawadzki RJ (2012) Complex conjugate artifact-free adaptive optics optical coherence tomography of in vivo human optic nerve head. Journal of Biomedical Optics 17(12):1–6 6
30. Ohmi M, Tanizawa M, Fukunaga A, Haruna M (2005) In-situ Observation of Tissue Laser Ablation Using Optical Coherence Tomography. Optical and Quantum Electronics 37(13):1175–1183. https://doi.org/10.1007/s11082-005-4189-2
31. Adegun OK, Tomlins PH, Hagi-Pavli E, Mckenzie G, Piper K, Bader DL, Fortune F (2012) Quantitative analysis of optical coherence tomography and histopathology images of normal and dysplastic oral mucosal tissues. Lasers in Medical Science 27(4):795–804. https://doi.org/10.1007/s10103-011-0975-1
32. Gallwas J, Stanchi A, Ditsch N, Schwarz T, Dannecker C, Mueller S, Stepp H, Mortensen U (2015) Effect of optical clearing agents on optical coherence tomography images of cervical epithelium. Lasers in Medical Science 30(2):517–525. https://doi.org/10.1007/s10103-014-1674-5
33. Mandurah MM, Sadr A, Bakhsh TA, Shimada Y, Sumi Y, Tagami J (2015) Characterization of transparent dentin in attrited teeth using optical coherence tomography. Lasers in Medical Science 30(4):1189–1196. https://doi.org/10.1007/s10103-014-1541-4
34. Olesen UH, Mogensen M, Haedersdal M (2017) Vehicle type affects filling of fractional laser-ablated channels imaged by optical coherence tomography. Lasers in Medical Science 32(3):679–684. https://doi.org/10.1007/s10103-017-2168-z
35. Rajabi-Estarabadi A, Bittar JM, Zheng C, Nascimento V, Camacho I, Feun LG, Nasiriavanaki M, Kunz M, Nouri K (2019) Optical coherence tomography imaging of melanoma skin cancer. Lasers in Medical Science 34(2):411–420. https://doi.org/10.1007/s10103-018-2696-1